FOURIER AND NON-FOURIER MODELS FOR PHOTOEMISSION

F. Scarlat, M. Oane, Anca Scarisoreanu, Ecaterina Mitru
National Institute for Laser, Plasma and Radiation Physics - NILPRP, Bucharest, Romania
E-mail of corresponding author: scarlat.f@gmail.com

Abstract

This paper is a theoretical study on the photoemission properties of metallic photocathodes in the high intensity ultrashort laser pulse regime, using Fourier and non Fourier models. First of all the Fourier-model was used. Next an analysis of the electron gas heating phenomenon and how this phenomenon leads to coupled heat equations (two temperature models) was conducted. The authors also tried to show that it is possible to use, in the second approximation, a non-Fourier model instead of two temperature models, using a single temperature hypothesis (the electron gas temperature equals the lattice temperature). The distributions for the thermal fields and photocurrents function of space, time, laser-intensity, incident angle and relaxation time are also represented.

INTRODUCTION

Free electron lasers (FELs) operate over a large portion of the electromagnetic spectrum, i.e.from a μ-wave to the VUV. At the high frequency end of the spectrum, FEL operation is severely limited by a number of factors, among which the transverse beam emittance, which is invers proportional with the square root density current. A high electron density implies not only a high peak current but also a low rms normalized emittance, ε_n. For example, in the case of X-FEL projects, ε_n[mm.mrad] has the values: 1.4 - XFEL [1], 1.2 - LCLS [2] and 0.85 - SCSS [3]. Recent development in the tehnology of photemissive electron sources offer promising advances over the conventional electron injectors [4], [5].

All photo-injector concepts share a drive laser which produces short bunches of photons and a photocathode which converts the photon bunch into short bunches of electrons [6], [7]. Photoemission from photo-cathodes is possible when the work function (or potential barrier, $e\Phi$) of the material is less than the photon energy ($\hbar\omega$) used, by at least: 1 eV if the material is a metal (in this case electrons are extracted from the conduction band) and 2 eV if the material is a semiconductor (electrons are here extracted from the valence band).

A photocathode is characterized by four parameters: quantum efficiency (QE), maximum laser wavelength (λ_m), life time (τ) and its ability to sustain a high electric field (E). For FEL nano-Coulomb pulses in picosecond time are required. The advantages of photoemission are the followings: high peak current density (> 100 A); fast time response (picosecond to femtosecond) and possibility to generate polarized electrons. As drawbaks: the need for very good vacuum, limited lifetime (few month) and very expensive (vacuum systems & laser). Metal cathodes have poor QE but are robust ($\tau \sim$ years).

Alcaline cathodes have good QE but are delicate and they need very good vacuum conditions < 10^{-10} torr. Starting from the above considerations as well as the NUCLEU program [8] for to conduct studies by means of the Nd:YAG laser system with 50 mJ at 1064 nm, 24 mJ at 532 nm, 8 mJ at 355 nm and 4 mJ at 266 nm, this paper represents a start in the metal photocathode studies using Fourier and non Fourier models for photoemission [9].

FOURIER MODELS

Fourier model starting from the basic Fourier heat equation, represented the input of our models [10]

$$\frac{\partial^2 T}{\partial x^2}+\frac{\partial^2 T}{\partial y^2}+\frac{\partial^2 T}{\partial z^2}-\frac{1}{\gamma}\frac{\partial T}{\partial t}=-\frac{Q(x,y,z,t)}{K}, \qquad (1)$$

where K - the thermal conductivity of the sample; γ - the thermal diffusivity of the sample ($\gamma = k/c\cdot\rho$); c -the heat capacity of the sample; ρ - the mass density of the sample. $Q(x, y, z, t)$ represents the heat rate (per volume and time unit) produced by the laser in the solid sample.

Based on Spatial Transform and Laplace Transform, the eigenfunctions from the standard theory and the eigenvalues from the boundary conditions were determined.

So for the proposed device a parallelepiped solid sample with dimensions a, b, and c was considered.
Considering a linear heat transfer (h – heat transfer coefficient) at the sample surface (the "radiation" boundary condition), we have:

$$\left[\frac{\partial K_x}{\partial x}-\frac{h}{K}K_x\right]_{x=-\frac{a}{2}}=0;\left[\frac{\partial K_x}{\partial x}+\frac{h}{K}K_x\right]_{x=\frac{a}{2}}=0, \qquad (2)$$

$$\left[\frac{\partial K_y}{\partial y}+\frac{h}{K}K_y\right]_{y=-\frac{b}{2}}=0;\left[\frac{\partial K_y}{\partial y}+\frac{h}{K}K_y\right]_{y=\frac{b}{2}}=0, \qquad (3)$$

$$\left[\frac{\partial K_z}{\partial z}+\frac{h}{K}K_z\right]_{z=-\frac{c}{2}}=0;\left[\frac{\partial K_z}{\partial z}+\frac{h}{K}K_z\right]_{z=\frac{c}{2}}=0. \qquad (4)$$

The semi-analytical solution to Fourier equation is:

$$\Delta T(x,y,z,t)=\sum_{i=1}^{\infty}\sum_{j=1}^{\infty}\sum_{o=1}^{\infty}a(\alpha_i,\beta_j,\chi_o)\cdot$$

$$\cdot b(\alpha_i,\beta_j,\chi_o,t)K_x(\alpha_i,x)K_y(\beta_j,y)K_z(\chi_o,z), \qquad (5)$$

where we have:

$$a(\alpha_i,\beta_j,\chi_o)=\frac{\alpha I_{ox}}{KC_iC_jC_o}\int_{-\frac{a}{2}}^{+\frac{a}{2}}e^{-\alpha x}K_x(\alpha_i,x)dx\cdot \tag{6}$$

$$\cdot\int_{-\frac{b}{2}}^{+\frac{b}{2}}\int_{-\frac{c}{2}}^{+\frac{c}{2}}e^{-2\left(y^2+z^2\right)/w_{ox}^2}K_y(\beta_j,y)K_z(\chi_0,z)dydz,$$

$$b(\alpha_i,\beta_j,\chi_0,t)=\frac{1}{\alpha_i^2+\beta_j^2+\chi_o^2}\left[1-e^{-\gamma_{ijo}^2t}-\right. \tag{7}$$

$$\left.-\left(1-e^{-\gamma_{ijo}^2(t-t_o)}\right)h(t-t_0),\right.$$

and

$$\gamma_{ijo}^2=\gamma\left(\alpha_i^2+\beta_j^2+\chi_o^2\right). \tag{8}$$

The photocathode employed for the study is 4 mm x 10 mm for a Kerst injector. Using a laser of the intensity (I_{0x}) plotted in Fig.1, by means of equations (5), (6), (7) and (8), some thermal distributions in different situations were plotted.

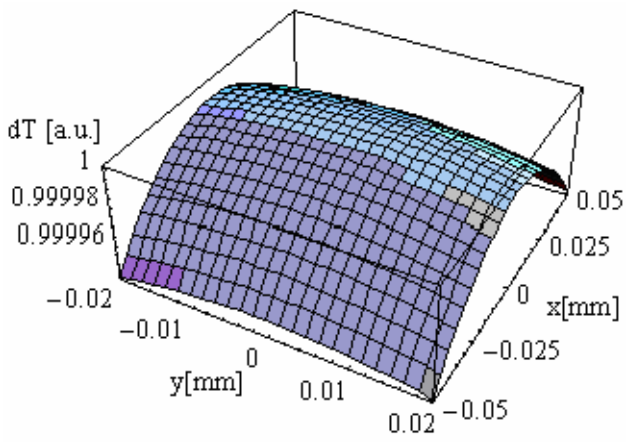

Figure 1: TEM_{00} classical laser field.

Fig. 2 presents the temperature generated by the cathode surface when the incident laser beam acts in TEM_{00} mode

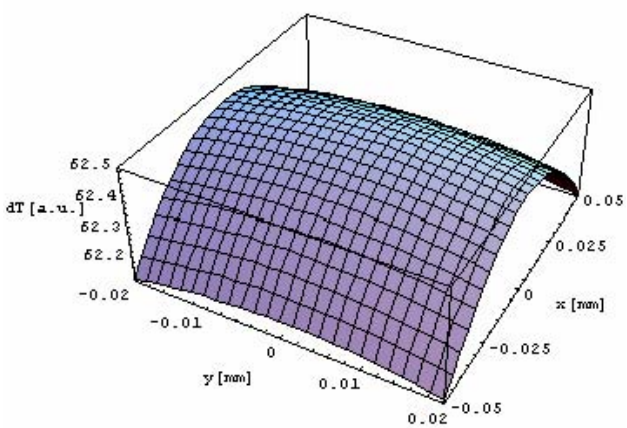

Figure 2: Photocathode temperature.

The thermal fields versus the incident angle of the laser beam are given in Fig.3.

If there is no vacuum than at the margins of the photocathode temperature decreases.

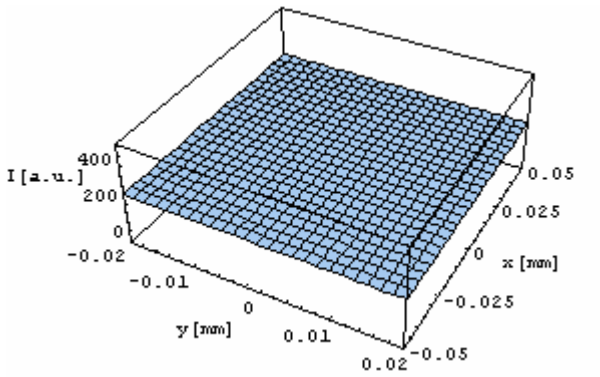

Figure 3: The thermal field produced by a flat laser beam.

The spatial distribution of the thermal field for a given incident angle and a flat laser beam (Fig. 4) when vacuum around the photocathode exists, is presented.

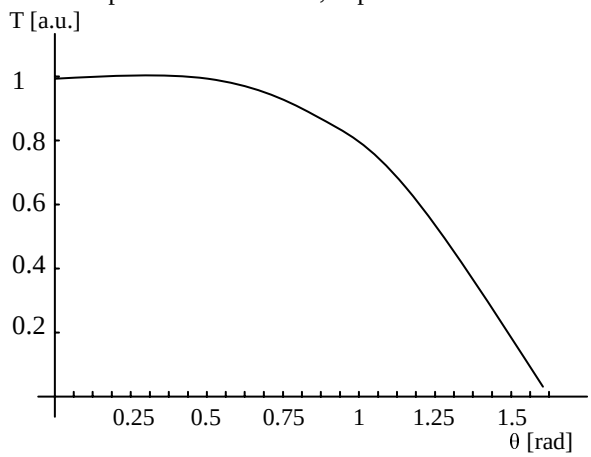

Figure 4: Photocathode temperature vs. the laser incidence angle.

THE NON-FOURIER MODELS

The Fourier model [10] contains several inconsistent implications. The most important is that the model implies an infinite speed of heat propagation.

The non Fourier Models start from the non-Fourier heat conduction equation:

$$\frac{\tau_0}{\alpha}\frac{\partial^2T}{\partial t^2}+\frac{1}{\alpha}\frac{\partial T}{\partial t}=\frac{\partial^2T}{\partial x^2}+\frac{1}{\lambda}\left[Q(x,t)+\tau\frac{\partial Q}{\partial t}\right], \tag{9}$$

where a, λ, τ_0 are thermal diffusivity, thermal conductivity, and relaxation time of the medium.

One of the models is the Anisimov model or the two-temperature model [11]. The coupled differential equations relating the electron temperature T_e to the lattice temperature T_i are given by the equations (10) where g represents the connection between electrons and

lattice; C and K are the heat capacities and thermal conductivity respectively:

$$C_e \frac{\partial}{\partial t} T_e = \frac{\partial}{\partial z}\left[k(T_e, T_i) \frac{\partial}{\partial z} T_e \right] - g(T_e - T_i) + I(z,t),$$

$$C_i \frac{\partial}{\partial t} T_i = g(T_e - T_i). \qquad (10)$$

Instead of the above model, the hyperbolic heat equation was used; assume that: $T_e = T_i$, which is valid when the puls length is comparable to the relaxation time and the electron temperature is higher than the lattice temperature.

Assume a sample with the thickness L with initial temperature distribution $T(x,0) = T_0$. Starting with the time $t = 0$ the front surface of the sample is irradiated by a laser-pulse with the laser pulse of energy intensity:

$$Q(x,t) = \begin{cases} \frac{Q_0}{\Delta x}\left(\frac{t}{t_p}\right)\exp(-t/t_p) & , 0 \le x \le \Delta X, \\ 0 & , \quad \Delta X \le x \le L, \end{cases} \qquad (11)$$

where t_p denotes the time duration of the pulse, Q_0 is the total energy intensity of a single pulse. According to common theory, Δx is corresponding to the skin depth of electromagnetic waves penetrating into the surface of the sample, L is the thickness of the medium.

The boundary conditions are:
$\partial T(0,t)/\partial x = 0$, $\partial T(L,t)/\partial x = 0$ and the initial conditions are: $T(x,0)=T_0$ and $\partial T(x,0)/\partial t = 0$.
Suppose that: $T_e=T_i$, than the solution is the following:

$$T_e(z) = T_0 + [T_e(0)-T_0]\exp(-z/L), \qquad (12)$$

where: $L = n(\hbar k_F/m)\tau$ with: k_F - the Fermi momentum and the factor n given the electron scattering will mimic a random walk – should be on the order of the square root of the ratio of the laser pulse time scale with the scattering time scale, or $n = (1\ ns/0.1\ ps)^{1/2} \approx 100$. τ is the relaxation time. The plot is presented in Fig. 5.

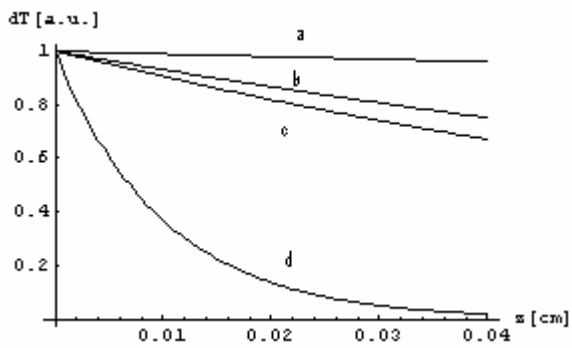

Figure 5: The temperature distribution versus depth in a Non Fourier model: the first curve, which is close to unity, is for the relaxation time 10^{-3} s (a), the others are for 10^{-6} s (b), 10^{-9} s (c) and 10^{-12} s (d).

LIMITS OF THE TWO MODELS

The shorter the relaxation time, the two different models (Fourier and non Fourier) would give the same results. It is obvious that the classical treatment is more powerful than the Quantum Mechanics models for this case of laser-solid interaction. The temperature field depends on the incident angle. The experiments shows that Fourier model is valid up to 10^{-6} s and the non Fourier model is valid up to 10^{-9} s.

Our simulations strongly suggest that all the phenomena are taking place at the sample surface rather than in the volume. Also our simulations prove that the higher the vacuum, the higher the temperature field is. ($A(x,y,z,t)=r_S \cdot \delta(z)$; $\delta(z)$ - Dirac Function).

EXAMPLES

Fig. 6 is a plot of the current densities vs temperature for different photocathodes.

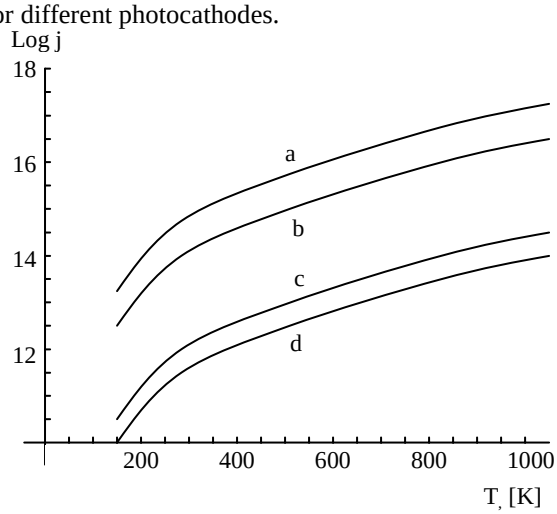

Figure 6: Variation of the current density vs temperature for: bright tungsten (a); lanthanum hexaboride (b), thoriated tungsten (c) and impregnated tungsten (d).

Fig. 7 presents the 3D (Cartesian coordinates) thermal fields for a laser beam heating the FEL photocathode at an angle of $\pi/4$. The laser beam is supposed to act in a Gaussian mode. The exposure time is 10^{-9} s. (Fourier model was used).

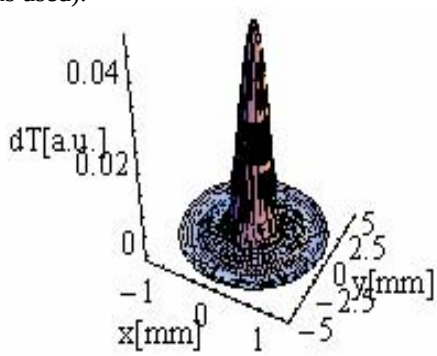

Figure 7: Thermal field for the exposure time of 10^{-9} s.

One can observe the edge effects due to the boundary conditions.

For nano and picoseconds exposure time, Figs. 8 and 9 (radial coordinates versus time) are suggestive. For femtoseconds exposure times the Fourier model breaks - down. In order to overcome the edge effect, it is possible to use the "state of the art" technologies regarding implantations of nano-particle (Au, Al, Ag, Cu, Ni) networks of 100 nm size, at 400 nm distance between them, on the photocathode edges.

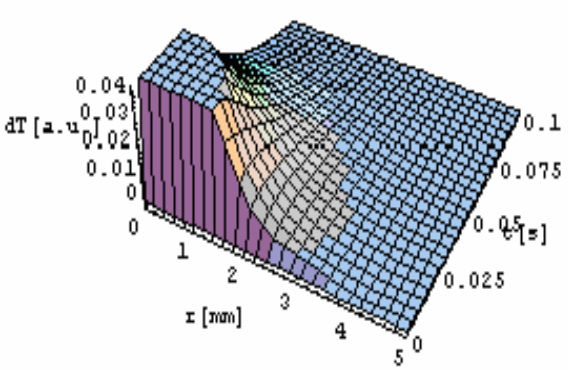

Figure 8: The thermal field for nano-seconds exposure time (radial coordinates versus time).

Table 1

Photocathode Material	Absorption coefficient (cm^{-1})
CsI	40
Au	0.77×10^6
Ag	0.83×10^6
Al	10^6
Cu	$16.6.10^6$
Ni	13.10^6

The big difference between the absorption coefficients (Table 1) of CsI, on one hand, and Al, Au, Ag, Cu, Ni on the other hand, makes our proposal realistic. For example, Fig. 9 presents the thermal field at the surface for a 100 nm diameter Au nano-particle which is at 400 nm depth. One can observe that the peak temperature is increased.

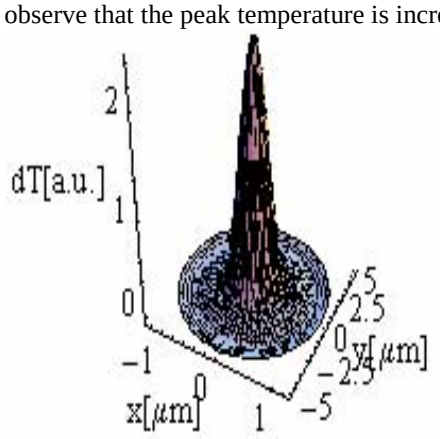

Figure 9: Thermal field at the surface for a 100 nm diameter Au nano-particle.

CONCLUSIONS

First of all Fourier models can offer useful information about the photochatode thermal field, especially when dealing with long a term pulses (μs) and powerful heating sources. In the range of picoseconds one has to take into account non-Fourier models, which imply a finite propagation speed of the thermal waves (in contrast with the Fourier models which involve infinite speed propagation). For non-Fourier models the problem to deal with is the relaxation time. If the heating pulse time is of the order of magnitude (or smaller) than the relaxation time, the differences between the two models are greater. In the range of femto- and atto- seconds one has to deal with a quantum heat transfer model. In fact the non-Fourier models are semi-classical models which take into account the quantum effects via the relaxation time (in an empirical style).

Another conclusion and a suggestion is that nano-particle networks, with a very high absorption coefficient, can improve the photochatode properties.

REFERENCES

[1]. M. Altarelli et al. (Eds.), The European X-Ray Free Electron Laser (XFEL), Technical Design Report, Preprint DESY 2006-097, DESY, Hamburg, 2006, (http://xfel.desy.de)

[2]. J. Arthur et al., Linac Coherent Light Source (LCLS). Conceptual Design Report, SLAC-R593 Stanford 2002 (http://www-ssrl.slac.stanford.edu/lcls/cdr).

[3]. Spring 8 Compact SASE Source (SCSS) X-FEL: Conceptual Design Report, RIEKEN, Japan, May 2005 (http://www-xfel.spring8.or.jp).

[4]. K. L. Jensen, D. W. Feldman, M. Virgo, P. G. O'Shea, "Measurement and analysis of thermal photoemission from a dispenser cathode", Phys. Rev. S.P.- Accelerators and Beams, 6, 083501,2003.

[5]. C. Travier, B. Leblond, M. Bernard, J.N. Kaila, P. Thomas, and P. Georges, Proceedings of the 1995 Particle Accelerator Conference, Vol.2, pp. 945-947, 1995.

[6]. G.R. Neil and L. Merminga, "Technical approaches for high-average-power free-electron lasers", Rev. Mod. Phys, 74, 685 - 699, 2002.

[7]. M. E. Couprie and J. M. Ortega, "Free-electron lasers sources for scientific applications", Analysis 28, pp.725-736, 2000.

[8]. F. Scarlat, M. Oane, A. Scarisoreanu, E. Mitru, "Testing Stand for Experimental Studies on Photocathode Materials", PN06 360503 NILPRP Program, 2006.

[9]. D.W. Tang, N. Arald, "Analytical solution of non-Fourier temperature response in a finite medium under laser-pulse heating", Heat and Mass Transfer 31 (1996) 359, Springer - Verlag, 1996.

[10]. M. Oane, Shyh - Lin Tsao, F. Scarlat, "Temperature field distribution in multi-layered solid media interaction", Optics & Laser Technology, Vol.39, Nr.1, Pg. 179 - 181, February 2007.

[11]. S. I. Anisimov, V.A. Khoklov, "Instabilities in Laser-Matter Interaction", Boca Raton", FL: CRC, 1995.